On the Enhancement and Suppression of Turbulent Wall Pressure by the Large Eddy Break Up Devices

T.P. Chong[1] and C. Muhammad[1]
Department of Mechanical and Aerospace Engineering, Brunel University London, Uxbridge, UB8 3PH, United Kingdom

(*Electronic mail: t.p.chong@brunel.ac.uk)

(Dated: 8 March 2024)

An experimental study is presented on the application of Large Eddy BreakUp (LEBU) on a flat plate as a source-targeting device to perturb the wall pressure fluctuations of a turbulent boundary layer. When interacting with a LEBU wake, the wall pressure spectra can establish a self-similar behaviour against s', which is a normalised separation distance between the LEBU's trailing edge and the targeted location for aeroacoustics noise source mitigation. It is found that $s' > 3$ is needed to achieve an overall reduction in the wall pressure fluctuations. The fundamental mechanism by which the LEBU can reduce the wall pressure fluctuation is investigated by studying the spatio-temporal evolution of turbulent spots. When the emanated LEBU wake is interacted with the outer part of turbulent spot, the shielding effect can always inhibit the turbulent fluids ejection from the spot's leading edge. However, incursion of the high momentum fluids wall-sweeping event at the spot's trailing edge can only be effectively prevented when $s' > 3$.

I. INTRODUCTION

Far field broadband radiation originated from turbulence scattering at a geometrical discontinuity, such as the trailing edge, represents a notorious engineering by-product. The scattering mechanism will be the most efficient when the trailing edge is completely orthogonal to the direction of the incoming flow. This is because the acoustical scattering at the straight edge will result in virtually no streamwise phase difference within the same spanwise plane of individual turbulent eddy. Hence, one of the effective strategies for the mitigation of the radiated turbulent broadband noise is to manipulate the streamwise scattering phases of the incoming turbulent eddies approaching the trailing edge to enable an *acoustic interference* mechanism[1,2]. This is commonly achieved by attaching a serration at the trailing edge, which will result in the presence of oblique edges relative to the inflow turbulent sources. Acoustical destructive interference can also be enforced in a trailing edge with a slit configuration[3] and structured porous surface[4]. Both configurations represent a targeted approach to gives rise to a frequency-tuning capability for the noise reduction.

Apart from the acoustic interference mechanism, self-noise reduction can also be achieved by a *source targeting* approach through reduction of the wall pressure fluctuations. Riblets have been shown to be able to slightly reduce the wall pressure power spectral density level at the low and high frequencies, but could cause an increase at the mid frequency[5]. When executing the source targeting at the outer part of turbulent boundary layer, mounting finlets near the trailing edge has been shown to significantly alter the turbulent boundary layer structure, and subsequently reduce the radiated noise level[6,7]. It is generally accepted that the finlet performance is mainly accredited to the sheltering of the trailing edge from large turbulent structures, where the shielding effect is sensitive to the ratio between the finlet height and boundary layer thickness.

Finlet, however, could be prone to generating higher parasite drag due to the accumulation of extra wetted area attaching to the surface. This raises a question of whether a method exists to reduce the wall pressure fluctuations through source targeting, but without incurring excessive level of drag in the process. The Large Eddy Break Up (LEBU) device, which normally consist of a two-dimensional thin plate or aerofoil placed onto the outer part of a turbulent boundary layer, had created a buzz in the research community in the late 1970's due to the perceived capability of turbulent skin friction reduction. Although a definite proof of net drag reduction remains inconclusive even after more than 40 years of research in this topic[8], LEBU is not expected to increase drag, if any, as significantly as the finlet. In addition, LEBU can exert beneficial effects in other applications. For example, the numerical results of Spalart *et al.*[9] suggest that LEBU has a potential to reduce the turbulent wall pressure fluctuations.

The wake emanated from the LEBU can disrupt the turbulence structure self-sustaining mechanisms of momentum transport into the boundary layer downstream. By targeting the large turbulent eddies in the boundary layer, interaction with the LEBU wake can break up the large structure into smaller, lower energy eddies that will eventually be dissipated by the viscosity[10]. Using a number of horizontal plates suspended over the flow surface, Hefner *et al.*[11] observe a 24% reduction of skin friction over a longitudinal range of 45 device heights. A net drag reduction, however, cannot be realised presumably due to the increased parasite drag incurred by the supporting struts of the LEBU. Derived from their velocity fluctuating spectra, Savill and Mumford[12] describe the process of small scale eddies penetration to the boundary layer via the wake of the LEBU, which also acts as a shield to prevent incursions of high speed fluid from the outer layer to the near wall region.

Although not exhaustive, the brief literature review conducted here on the LEBU's capability to break up the large turbulent structure suggests that it has a potential to execute an effective source targeting to achieve reduction in the turbulent wall pressure, which can lead to reductions in the self-noise and turbulent boundary layer noise radiation. This topic remains unexplored and scarce in the literature. The first objec-

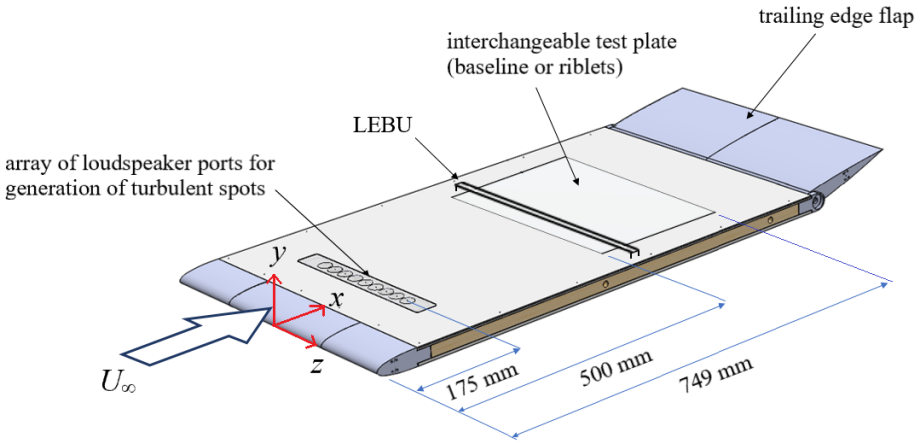

FIG. 1. Schematic showing the flat plate model used in the current study. The coordinate system is also shown. Drawing is not to scale.

tive of this paper, therefore, is to investigate the wall pressure spectra when the boundary layer is subjected to interaction with LEBU wake. The LEBU will be placed up to $8\delta_\circ$ upstream from the wall pressure reference location, where $\delta_\circ$ is the boundary layer thickness at the reference. Note that reducing turbulent skin friction by LEBU is not the main objective of this paper.

Turbulent spots are commonly regarded as the building block of a fully-developed turbulent boundary layer. Studying the structural change of an isolated turbulent spot after a physical impingement with the LEBU, as well as the interaction between the LEBU's emanated wake and the turbulent boundary layer, can provide a fundamental insight into the generation mechanisms of the turbulent wall pressure sources. This unique study, which represents the second objective of this paper, is facilitated by an active boundary layer tripping technique that can result in a controlled and periodic generation of turbulent spots in an otherwise laminar boundary layer, such as that developed by Chong and Juknevicius[13].

II. EXPERIMENTAL SETUP, MEASUREMENT AND ANALYSIS TECHNIQUES

The experiments were conducted in an open circuit, suction type wind tunnel where the axial fan is driven by a 7.5 kW motor capable of achieving velocity up to 35 $\mathrm{m\,s^{-1}}$ inside the 0.5×0.5 m working section. The walls are constructed by Perspex to allow optical access. The mean turbulence intensity of the flow is measured to be less than 0.5%.

A. Design of a flat plate system with LEBU

The flat plate system developed in Muhammad and Chong[5] is also employed here for the study of LEBU. As shown in Figure 1, the coordinate system is represented by x, y and z, which denotes the streamwise, wall-normal and lateral directions, respectively. In the figure, $x = 0$ refers to the leading edge of the flat plate. The flat plate contains a recess between $500 \leq x \leq 749$ mm for an instrumented test plate with microphones, which facilitates the measurement of wall pressure fluctuations. A trailing edge flap is used to control the front stagnation point to ensure a smooth boundary layer development on the upper flow surface. When a fully developed turbulent boundary layer is required, a zig-zag type turbulator will be placed at the same location as the loudspeaker strip, $x = 175$ mm, to serve as a passive device to artificially generate a two-dimensional turbulent boundary layer.

An illustration of the LEBU system is shown in Figure 2. The LEBU is a NACA0014 symmetrical aerofoil with chord length C_{LEBU} = 15 mm, which entails a maximum thickness of approximately 2 mm to resemble a thin, but also sturdy device. The LEBU is supported by struts that are laser-cut from 0.5 mm thick plywood. The height of the strut used here ensures that the centreline and trailing edge of the LEBU is raised to a height of $\tilde{h}$ = 5.0 mm above the surface of the flat plate. The struts carrying the entire LEBU are movable in the streamwise direction from the reference location X_{ref}, which is at $x = 625$ mm. The distance between the LEBU's trailing edge and the reference location is denoted by s, as depicted in Figure 2. In this study, there are total of five s tested against three freestream velocities $U_\infty = 10, 12$ and 15 $\mathrm{m\,s^{-1}}$. In what follows, s will be non-dimensionalised by the boundary layer thickness at X_{ref}, resulting in $s' = s/\delta_\circ$. Both the dimensional and non-dimensional tabulated values can be found in Table I.

B. Instrumentation

The Knowles FG3229-P07 electret microphones, which are circular (2.57 mm diameter) with a sensing diameter of 0.8 mm, are used in the wall pressure fluctuation measurements. As shown in Figure 3, the microphone is mounted remotely underneath the wall surface with an acrylic holder. It is connected to the wall surface via a 40 mm silicone tube. The

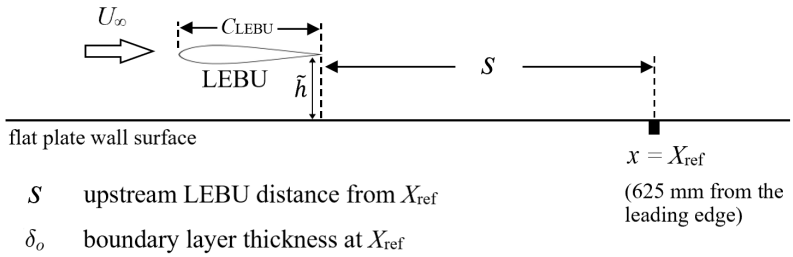

FIG. 2. Schematic showing the LEBU arrangement. Drawing is not to scale.

s (mm)	5	15	30	50	80
s' at 10 m s^{-1}	0.440	1.321	2.643	4.405	7.047
s' at 12 m s^{-1}	0.461	1.382	2.763	4.605	7.369
s' at 15 m s^{-1}	0.476	1.428	2.856	4.761	7.617

TABLE I. Dimensional (s) and non-dimensional ($s' = s/\delta_\circ$) distances of the LEBU's trailing edge placement in the upstream direction from X_{ref}. Note that $\delta_\circ = 11.35$, 10.86 and 10.50 mm for $U_\infty = 10, 12$ and 15 m s^{-1}, respectively

.

same type of silicone tube of about 3 m long is connected to the other end of the acrylic holder, which will come out from the working section of the wind tunnel. The use of a long tube at the other end is to ensure that the acoustic waves travelling inside the remote microphone system does not encounter a sudden termination that will result in the backward reflection. If this is not avoided, standing waves will be formed inside the remote microphone system that could result in some spurious fluctuations in the power spectral density. The same principle of remote microphone configuration for turbulent wall pressure fluctuations measurement has been adopted by others[14–16]. The current remote microphone configuration ensures that the 0.4 mm pinhole diameter of the wall surface will also be maintained as much as possible throughout the tubing system of the remote microphone. For the tube connecting the wall surface to the acrylic holder, care is taken to ensure minimal curvature and bend to minimise the pressure loss.

During the experiment, the raw data from the remote microphone is sampled at a rate of 40 kHz for 15 seconds, which amounts to 600,000 samples. The data acquisition system has a 16-bit resolution and each sampling channel has a built-in anti-aliasing filter.

The flow velocity fluctuation is measured by a miniature single hot wire (Dantec 55P11), which consists a 1.25 mm long, 5 μm diameter tungsten sensing wire. Operated by a constant temperature anemometer, the overheat ratio of the hot wire is set to 1.8, which will facilitate an operating temperature of the hot wire to be approximately 300^{o}C. The hot wire is attached to a three-axis traverse system, in which the step motors are capable of achieving very fine movement of 0.01 mm. Such a high spatial resolution in the traverse is suitable for the boundary layer measurement. The analogue-to-digital (A/D) card used in the hot wire acquisition has a 12-bit resolution. The data sampling rate is set at 20 kHz for 13 seconds for the tripped turbulent boundary layer (results presented in Section III). The sampling time increases to 26 seconds for the turbulent spot case (results presented in Section IV). The doubling of sampling time is to ensure that each measurement point contains adequate number of individual turbulent spot signatures (approximately 80) to achieve an acceptable level of convergence for the ensemble averaging. In both the passively-tripped and actively-triggered cases in the generation of turbulent boundary layer, a low-pass filter of 10 kHz is utilised in the data acquisition to ensure that the sampled signal is inside the Nyquist frequency and is not contaminated by aliasing. Temperature correction of the sampled hot wire signals is performed during the post-analysis.

C. Generation of turbulent spots

Finally, some information about the generation of the turbulent spots, as well as their analysis methods, are discussed here. Referring to Figure 1, the turbulent spots are created artificially in an otherwise laminar boundary layer by injecting puffs of air through an 0.5 mm diameter orifice at $x = 175$ mm. Such turbulent spot generation method has been employed widely[17–19]. The small air jet is generated by driving the miniature loudspeaker at the middle of the strip, i.e. $z = 0$. A Teledyne T3AFG10 function generator is used to generate the square wave pulse signals with a 1 ms pulse width at a frequency of 3 Hz. This particular spot generation frequency is confirmed as the ideal value to ensure that interaction between individual spot does not occur for the entire measurement points, and at the same time not resulting in excessive overall sampling time required. The data analysis of the turbulent spot in this paper relies on the ensemble averaging technique. To perform the ensemble averaging success-

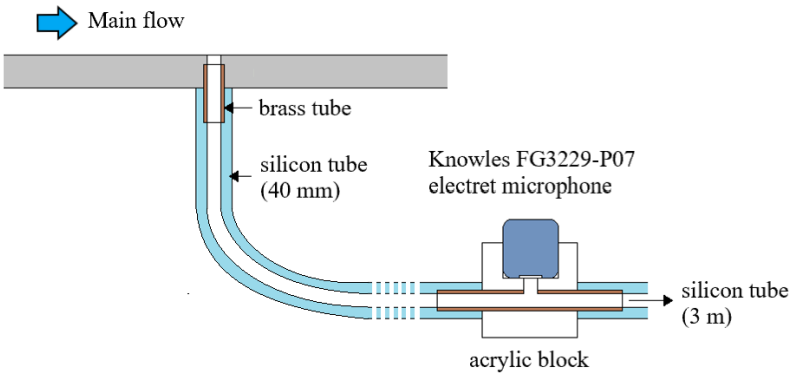

FIG. 3. The remote microphone configuration (cross section view).

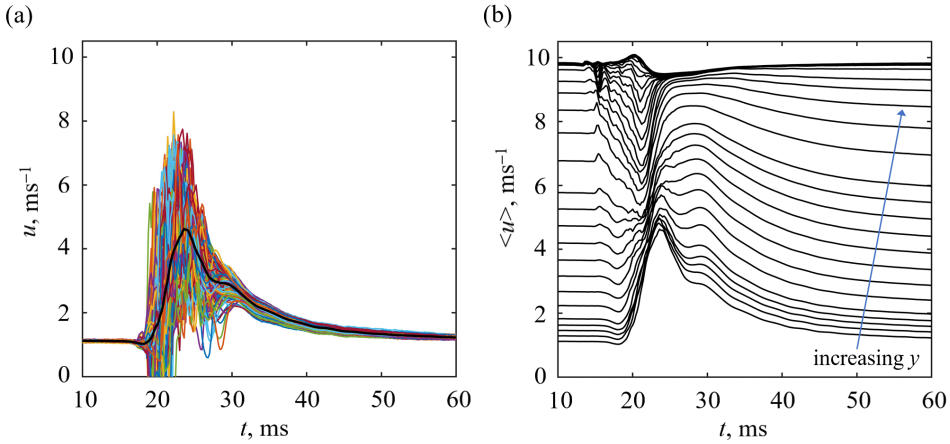

FIG. 4. (a) An ensemble of velocity signals (colour lines) produced by 341 turbulent spots. The black solid line is the ensemble phase-averaged velocity $\langle u \rangle$, and (b) ensemble phase-averaged velocity signatures for a boundary layer, where each line represents the velocity measurements taken at different y locations from the wall surface. This example is taken from Chong and Juknevicius[13].

fully, the rising edge of each input pulse signal can be set as the time of origin ($t = 0$ ms) of an individual spot event. This allows the generation of an ensemble of velocity fluctuations, which is shown in Figure 4(a) from data obtained in Chong and Juknevicius[13] as an example. Note that this example is in the absence of the LEBU. The ensemble is then averaged to obtain the mean velocity time signature $\langle u(x,y,t) \rangle$, which is represented by the thick black line in the figure. Typical mean velocity signatures at various y locations measured across a boundary layer is shown in Figure 4(b). The velocity perturbation caused by an ensemble-averaged turbulent spot is given by:

$$\tilde{u}(x,y,t) = \frac{\langle u(x,y,t) \rangle - U_{\text{LEBU on}}(x,y)}{U_\infty(x)}, \qquad (1)$$

where $U_{\text{LEBU on}}(x,y)$ is the local velocity in the laminar boundary layer, which is subjected to the perturbation by the LEBU wake but without the presence of turbulent spots. The velocity perturbation $\tilde{u}(x,y,t)$ defined above therefore quantifies the momentum excess or deficit produced by the ensemble-averaged turbulent spot under an already perturbed laminar boundary layer. This special definition for the velocity perturbation can extract and discard the component of the LEBU wake, which is stationary in the time domain velocity signals.

The root-mean-square (r.m.s) velocity fluctuation of the turbulent spot normalised by the local freestream velocity at a corresponding time instance can be given by:

$$u'(x,y,t) = \frac{\sqrt{\frac{1}{N}\sum_{i=1}^{N}\left[u_i(x,y,t) - \langle u(x,y,t) \rangle\right]^2}}{U_\infty(x)}, \qquad (2)$$

where N is the total number of turbulent spots measured. Note that the $u'(x,y,t)$ already contains normalisation by the local freestream velocity $U_\infty(x)$. Therefore, it is a measure of the turbulence intensity caused by the passage of a turbulent spot.

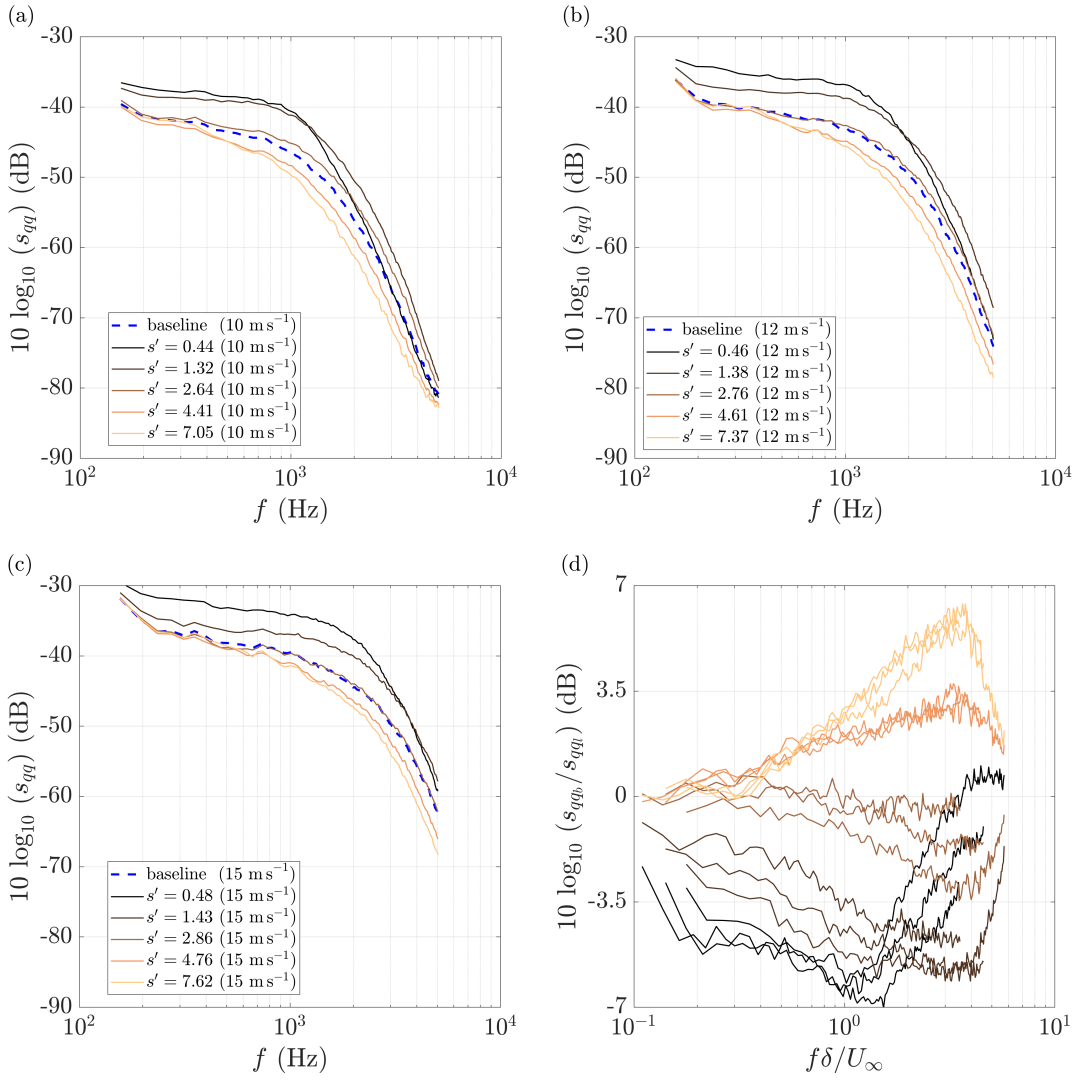

FIG. 5. Fluctuating wall pressure spectra s_{qq} at X_{ref} for U_∞ = (a) 10 ms^{-1}, (b) 12 ms^{-1} and (c) 15 ms^{-1}. (d) Difference in the fluctuating wall pressure spectra between the baseline s_{qqb} and those subjected to the LEBU s_{qql} measured across $0.44 \leq s' \leq 7.62$. This sub-figure represents a collection of spectra pertaining to U_∞ = 10, 12 and 15 ms^{-1} at X_{ref}.

III. WALL PRESSURE FLUCTUATIONS AT X_{ref} SUBJECTED TO LEBU AT VARIOUS s'

The measurement campaign includes experiments conducted at three freestream velocities, U_∞ = 10, 12 and 15 ms^{-1} to facilitate a sensitivity study for the streamwise distribution of LEBU in s' for their effect to the wall pressure turbulent noise sources production. For U_∞ = 10, 12 and 15 ms^{-1}, the LEBU entails $\tilde{h}u_\tau/\nu \approx 170$, 200 and 240, and $\tilde{h}/\delta_\circ \approx 0.44$, 0.46 and 0.48, respectively. Hence, the LEBU is targeting the outer region of turbulent boundary layer at X_{ref}. Note that ν is the kinematic viscosity, and u_τ is the friction velocity determined by the Clauser method from the measured baseline velocity profiles at X_{ref}.

The power spectral density of the wall pressure fluctuations, s_{qq}, will now be examined. Figure 5(a−c) shows the s_{qq} spectra across a range of s' at U_∞ = 10, 12 and 15 ms^{-1}, respectively. The baseline s_{qqb} refers to the spectra when LEBU is not used. It is clear that installing LEBU can change the wall pressure spectra at X_{ref} significantly. More importantly, locating the LEBU too close to X_{ref} (i.e. $s' < 1.43$) is shown to increase the amplitude of the wall pressure spectral across almost the entire range of frequency presented in the figure. There seems to be an intermediate separation distance ($2.64 < s' < 2.86$) where the wall pressure spectra is not affected too much by the presence of LEBU. Beyond that, the wall pressure fluctuations at X_{ref} begin to be suppressed across the entire range of frequency. This is a significant outcome because it suggests that having a spatially more developed LEBU wake (when s' is sufficiently large) is more effective in the suppression of the large scale turbulence than having a LEBU placed at low s' whose wake is narrow and has a larger level of velocity deficit. This phenomenon will be discussed

further in Section IV. It is important to note that the wall pressure fluctuations might be reduced further at $s' > 7.62$ as inferred by the trends exhibited in Figure 5(a−c). However, this remains to be confirmed in the future studies.

Figure 5(d) shows a collection of spectra pertaining to the difference in wall pressure fluctuations between the baseline, s_{qqb} and those subjected to the LEBU, s_{qql}. The frequency is non-dimensionalised by $U_\infty/\delta_\circ$, where $\delta_\circ$ is the local boundary layer thickness at X_{ref}. A positive value of the $10\log_{10}(s_{qqb}/s_{qql})$ denotes a reduction of wall pressure power spectral density level by the LEBU when compared to the baseline level, and vice versa. The $10\log_{10}(s_{qqb}/s_{qql})$ spectra provide a vivid representation in which the LEBU's very near wake interaction with the turbulent boundary layer can result in a significant enhancement of the wall pressure fluctuation as manifested by the predominantly negative $10\log_{10}(s_{qq_b}/s_{qq_l})$, and the weak recovery at the high frequency region.

The $10\log_{10}(s_{qqb}/s_{qql})$ spectra show signs of abatement when the LEBU is gradually shifted upstream. It is observed that the LEBU can only be effective for the mitigation of wall pressure fluctuations, i.e. $10\log_{10}(s_{qqb}/s_{qql}) > 0$, when $s' > 3$. Remarkably, the reduction in wall pressure fluctuations is effective across the entire frequency range investigated here. Another interesting observation is that the normalised frequency corresponding to the maximum wall pressure reduction always occurs at $f\delta_\circ/U_\infty = 3.5$.

Following the discussion of the spectral characteristics, the next step is to examine the overall wall pressure fluctuations S_{qql} subjected to the LEBU treatment. This quantity is obtained by integrating the wall pressure fluctuation over a large frequency range $\int_f p'_{qq} df$, which can also be regarded as the standard deviation of the wall pressure fluctuations. Figure 6 shows the variations of $10\log_{10}(S_{qqb}/S_{qql})$ against s' at several freestream velocities. Note that the S_{qqb} represents the overall wall pressure fluctuations for the baseline case. A high level of self-similarity behaviour can be achieved by the LEBU within the ranges of s' and U_∞ investigated here. Similarly, the onset of reduction for the overall wall pressure fluctuations is found to occur when $s' = 3$ is fulfilled. This represents a simple optimisation rule for the LEBU in the mitigation of wall pressure fluctuations at zero pressure gradient flow.

IV. INTERACTIONS BETWEEN TURBULENT SPOTS AND LEBU WAKE AT X_{ref}

Boundary layer study has been performed at locations before, and after the "$s' = 3$" threshold to understand how it is established. Chong and Juknevicius[13] developed an experimental technique that can exploit the "deterministic" turbulent boundary layer concept to enable the study of aeroacoustics noise source mechanisms in the spatial and temporal domains. The principle is based on the *turbulent spot*, whose dynamic response after interaction with a LEBU's wake in an otherwise laminar boundary layer can be exploited to study some of the physical mechanisms that produce the results in the previous section. The advantage of this analysis method is that it can trace a detailed, ensemble-averaged turbulence flow field in both the space and time domains. The analysis performed here will focus on the most fundamental aspect, which is related to isolated turbulent spot that has not yet merged with others. The main quantities to be studied here are the velocity perturbations and turbulence intensity, both of which have been defined in Section II C.

The original turbulator at $x = 175$ mm is removed first to ensure that a laminar boundary layer can dominate much of the flat plate surface. The experiment was performed at $U_\infty = 7\ \text{m s}^{-1}$, which produces a boundary layer thickness of 5.6 mm at $x = X_{\text{ref}}$. After the removal of the turbulator, the single miniature loudspeaker at the middle of the strip becomes the primary source of boundary layer point disturbance that will lead to the generation of turbulent spots at downstream.

A. Turbulent spots developed on a baseline flat plate (i.e. without LEBU)

Figure 7(a) and (b) shows the velocity perturbation $\tilde{u}$ and turbulence intensity u' contours, respectively, pertaining to the turbulent spot's plane of symmetry at X_{ref} for the baseline flat plate. In the contours, the abscissa refers to the normalised time scale $t' = t/t_f$. $t = 0$ is the time of origin, which represents the instance when the miniature loudspeaker is triggered. t_f represents the time of flight for the turbulent spot to convect from the location of the miniature loudspeaker to X_{ref} at a prescribed convection velocity u_c. By referring to an earlier study from Chong and Zhong[20], the spot is found to propagate at $u_c \approx 0.72U_\infty$ under a zero pressure gradient flow. This value will be adopted here. The ordinate is the wall-normal distance normalised by the maximum thickness of the turbulent spot δ_{spot} measured at X_{ref}.

In Figure 7(a), the unperturbed laminar field is characterised by white region where $\tilde{u} \approx 0$. In order to depict the shape of the turbulent spot, thresholds of $\tilde{u} = \pm 0.04$ are applied in the contour. The ensemble-averaged turbulent spot displays four distinctive regions: (1) the near wall region that is dominated by the high level of *positive perturbations*, i.e. $\tilde{u} > 0$, and (2) the outer region where the velocity perturbations are predominantly *negative*. This reflects very well of a typical turbulent boundary layer velocity profile that exhibits near wall velocity excess and outer layer velocity deficit. At some intermediate heights from the surface, the turbulent spot will encounter both positive and negative perturbations along the time of flight. These intermediate heights also coincide with the (3) *leading edge overhang* of the turbulent spot. Here, the leading edge overhang is formed by the upstream 'ejections' of turbulent fluid with sufficient energy from the near wall region to beyond the edge of the laminar boundary layer. Although the ejected turbulent fluid propagates faster than the main body of the turbulent spot, it has no self-regeneration mechanism outside the boundary layer so it will gradually decay and join the nose of the turbulent spot to form an overhang. Another important feature pertaining to a turbulent spot that is discernible from the velocity perturbation contour is the presence of a (4) *becalmed region* that corresponds to a slow

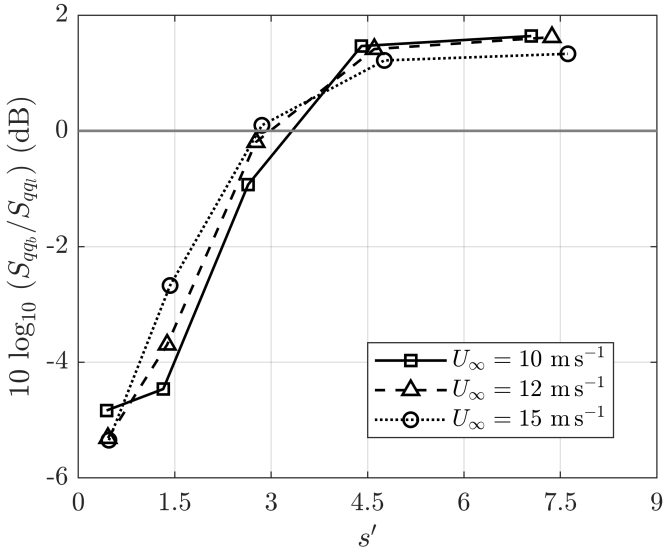

FIG. 6. Difference in the overall fluctuating wall pressure between the baseline S_{qq_b} and those subjected to the LEBU S_{qq_l} as a function of s'.

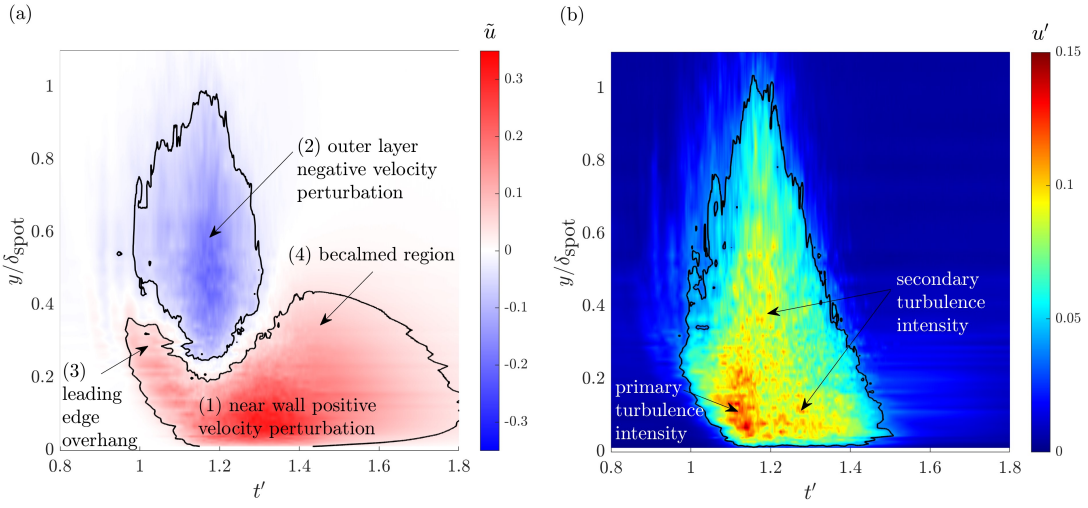

FIG. 7. Contours of the baseline (a) velocity perturbation $\tilde{u}$, and (b) turbulence intensity u', at the plane of symmetry of a turbulent spot at $x = X_{\text{ref}}$.

recovery of velocity behind each turbulent spot. The becalmed region is formed by the downstream 'sweeping' of high momentum fluid from the freestream towards the near wall of the turbulent spot's trailing edge. From the perspective of the velocity perturbation, it is difficult to distinguish the interface separating the becalmed region and the trailing edge of the turbulent spot. However, the becalmed region has a fuller velocity profile that is even more stable than the local laminar boundary layer profile. The overall shape of the velocity perturbation contour and their main features agree well with the literature[20–22].

Figure 7(b) shows the contour of the corresponding turbulence intensity. The turbulent spot delineated by the turbulence intensity, though well defined, is quite different from that delineated by the velocity perturbation. Nevertheless, the salient features such as the leading edge, including its overhang, the maximum height and the trailing edge are all distinguishable. As expected, the becalmed region is no longer discernible because by definition the turbulence intensity level at the becalmed region is very low. The leading edge at the near wall region, and underneath the overhang, are characterised by very high turbulence intensities between $10 \sim 14\%$. This region is herein called the *primary turbulence intensity*, which can also be found at other streamwise locations. The presence of a primary turbulence intensity within a turbulent spot is consistent with Gad-el-Hak *et al.*[23] and Glezer *et al.*[18] who observe that a strong destabilising regime is located at the leading edge interface under the overhang. This concentrated region is where the turbulence is produced, consistent with the earlier explanation of the near wall ejection of turbulent fluid

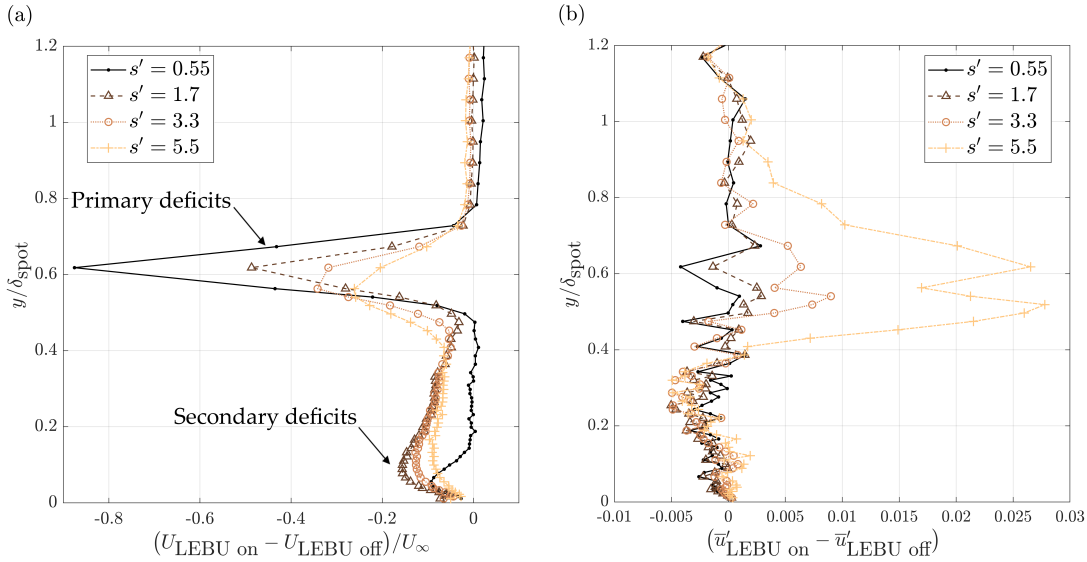

FIG. 8. Profiles of time-averaged ($0 \leq t' \leq 0.5$, i.e. before the arrival of turbulent spot) from ensembles of (a) velocity differences, and (b) turbulence intensity differences, at $x = X_{\text{ref}}$.

that will eventually lead to the formation of a leading edge overhang. The presence of the primary turbulence intensity is needed for the destabilisation of the surrounding laminar boundary layer. High and concentrated *secondary turbulence intensity* ($8 \sim 10\%$) is also found to encompass regions that would otherwise coincide with the prominent negative perturbation region (at the outer layer) and positive perturbation region (near wall).

Ultimately, the salient features pertaining to a canonical turbulent spot will be altered when it interacts with a LEBU wake at the outer layer. The dynamic responses as a result of the mixing between them could shed some lights on the physical mechanisms that produce some of the results discussed in Section III.

B. Interactions between the LEBU wake and laminar boundary layer (i.e. $t' < 0.5$)

The profiles of laminar boundary layer subjected to the LEBU wake, prior to the interaction with turbulent spots, are discussed in this section. Figure 8(a) shows the difference in mean velocity profiles, $\left(U_{\text{LEBU on}} - U_{\text{LEBU off}}\right)/U_\infty$, as a function of y/δ_{spot}. The first and second terms in the dividend denote the velocity measured with LEBU and without LEBU, respectively. Figure 8(b) represents the difference in turbulence intensity profiles $\left(\overline{u}'_{\text{LEBU on}} - \overline{u}'_{\text{LEBU off}}\right)$. Note that $\overline{u}'$ is obtained from the ensemble averaging method described in Equation 2, where the overbar denotes the mean turbulent profiles calculated between $0 \leq t' \leq 0.5$, which is prior to the arrival of the turbulent spot at X_{ref}. Note that $t' = 1$ corresponds to the non-dimensional time instance when the spot arrives.

It is also important to note that, in the current case where turbulent spots are generated in an otherwise laminar boundary layer, the streamwise separation distance between the LEBU's trailing edge and X_{ref} is normalised by the local turbulent spot thickness. Therefore, $s' = s/\delta_{\text{spot}}$.

In Figure 8(a), significant deficits occurs at $y/\delta_{\text{spot}} \approx 0.6$, which are directly caused by the mixing between the boundary layer and LEBU wakes. When the LEBU is placed at $s' = 0.55$, which is at the closest distance from X_{ref}, the level of deficit is the largest and the mixing layer is the narrowest in width. As s' increases to 1.7, the larger streamwise separation distance between the LEBU and X_{ref} alters the wake−boundary layer mixing and causes a reduction of the velocity deficit level. Further increases of s' to 3.3 and 5.5 will start to show an enlargement of the mixing layer width, and deviation of the mixing layer flight path as manifested by a downward induction towards the wall. Figure 8(b) demonstrates that the turbulent profiles corresponding to the primary deficit region are not affected significantly by the mixing if the LEBU is relatively nearby at $s' = 0.55$ and 1.7, where the levels are close to the baseline case (LEBU off). However, further increases of s' to 3.3 and 5.5 will lead to elevation of the turbulence intensity levels and they become much larger values than those produced by the baseline case. The dominance of the LEBU wake at large s' is manifested by the appearance of double peaks for the turbulence profiles, which is a common feature for wake turbulent profile developed in a non-viscous, potential flow. From the observations thus far, interactions between the laminar boundary layer and the LEBU wake at $s' = 0.55$ and 1.7 will produce the mean and turbulent velocity profiles that are relatively different compared to those when the LEBU is placed at $s' = 3.3$ and 5.5.

The LEBU wake can also induce secondary deficits at the near wall region of the laminar boundary layer profile, which are shown in Figure 8(a). The wall-normal distance of the secondary deficit, which varies with s', is denoted as y_2. At $s' = 0.55$, secondary deficit starts to emerge at $y_2/\delta_{\text{spot}} = 0.05$, where it is still spatially isolated from the primary deficit at

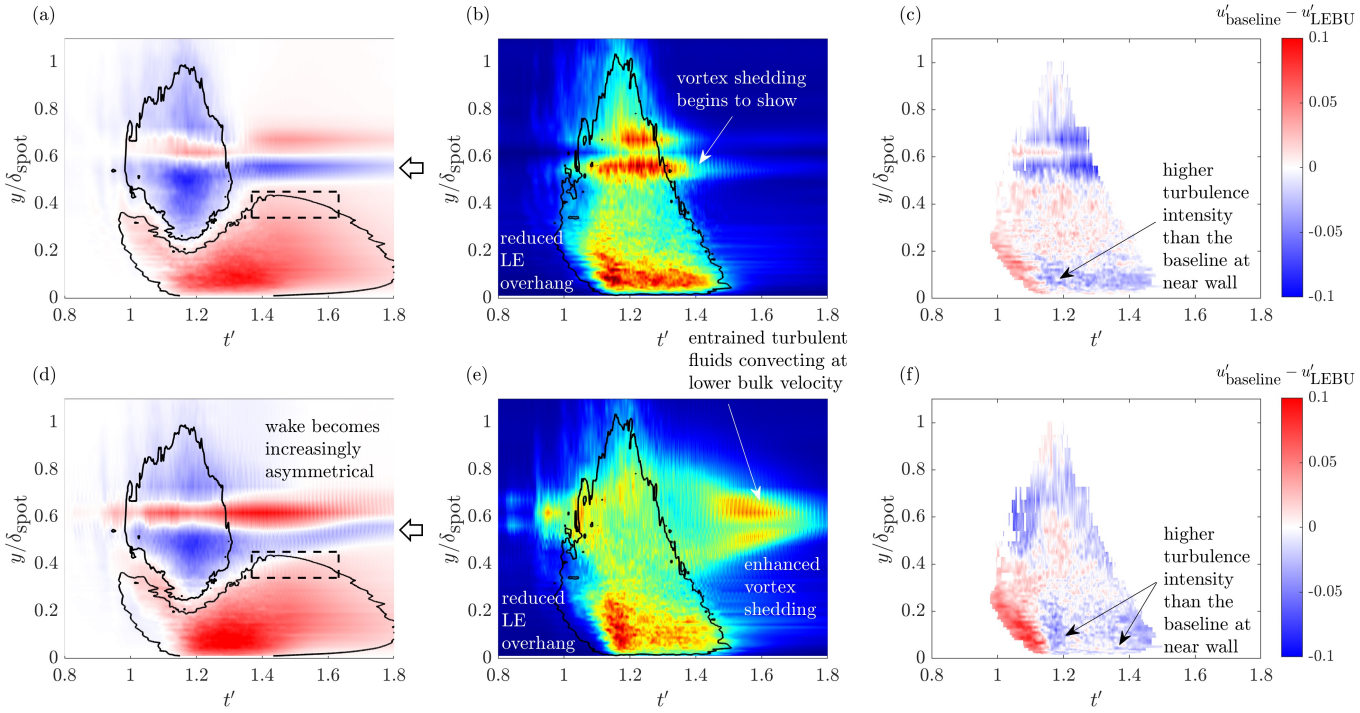

FIG. 9. Contours of the (a, d) velocity perturbation $\tilde{u}$, (b, e) turbulence intensity u' and (c, f) difference in turbulence intensity $u'_{\text{baseline}} - u'_{\text{LEBU}}$ at the plane of symmetry of a turbulent spot at $x = X_{\text{ref}}$. The LEBU is placed at $s' =$ (a−c) 0.55, and (d−f) 1.7. The outlines of the baseline (i.e. in the absence of LEBU) turbulent spot identified in Figure 7 are superimposed as black lines to the contours of (a, d) $\tilde{u}$ and (b, e) u'. Refer to Figure 7 for the colorbars of $\tilde{u}$ and u'.

$y/\delta_{\text{spot}} = 0.62$. However, as s' increases to 1.7, 3.3 and 5.5, their corresponding secondary deficits will be displaced further away from the wall surface to $y_2/\delta_{\text{spot}} = 0.07$, 0.08 and 0.09, respectively. This gives a linear function of $y_2/\delta_{\text{spot}} \propto 0.0052s'$ within $1.7 \leq s' \leq 5.5$. Note that there might be a coalescence activity between the primary and secondary deficits at some intermediate heights ($0.2 < y/\delta_{\text{spot}} < 0.4$).

The whole process suggests that direct interaction between the LEBU wake and laminar boundary layer at the primary deficit region can also induce a secondary momentum deficit at the near wall region. Also, the velocity deficit at the primary region does not directly correlate to the turbulence level, with the latter only starts to elevate at $s' > 3$.

C. Interactions between the LEBU wake and turbulent spots at $s' < 3$

Previously, in the self-similar study of the overall wall pressure fluctuations (Figure 6), it is shown that reduction of the overall wall pressure fluctuation by the LEBU wake can only be achieved when $s' > 3$. Below which, the opposite will occur. To understand the associated flow features, this section will study the interactions between the LEBU wake and turbulent spots when the overall wall pressure fluctuations increase, i.e. $s' < 3$. Later, in Section IV D, the focus will be on $s' > 3$ when reduction of the overall wall pressure fluctuations occurs.

Figure 9(a−c) show the contours of velocity perturbation $\tilde{u}$, turbulence intensity u' and difference in turbulence intensity $u'_{\text{baseline}} - u'_{\text{LEBU}}$, respectively, subjected to LEBU placement at $s' = 0.55$. These contours associate with the turbulent spot's plane of symmetry at X_{ref}. Similarly, the abscissa of the contours refers to the normalised time scale t', and the ordinate is the wall-normal distance normalised by the maximum thickness of the baseline turbulent spot δ_{spot}, which is also measured at X_{ref}. The outlines of the baseline (i.e. in the absence of LEBU) turbulent spot in the contexts of $\tilde{u}$ and u', as depicted in Figure 7, are also superimposed to the contours in Figure 9(a) and 9(b), respectively.

The definition in Equation 1 for the velocity perturbation $\tilde{u}$, which aims to extract the LEBU wake component from the turbulent spot, is manifested in Figure 9(a). It can be seen that the LEBU wake has been successfully extracted from the contour at $t' < 1$, i.e. before the arrival of the turbulent spots. At $t' > 1$, wake interaction with the turbulent spot between $0.5 < y/\delta_{\text{spot}} < 0.75$ results in some structural changes, most notably the appearance of $+\tilde{u}$, at the outer layer. The interaction then generates two prominent elongated streaks of opposite perturbation signs behind the turbulent spot. The appearance of these streaks is because the LEBU wake has now become the tracer of a mixing layer after interacting with the turbulent spot, which will be visible under the ensemble-averaging analysis conducted here.

The elongated streaks can be studied further by introducing coefficients of:

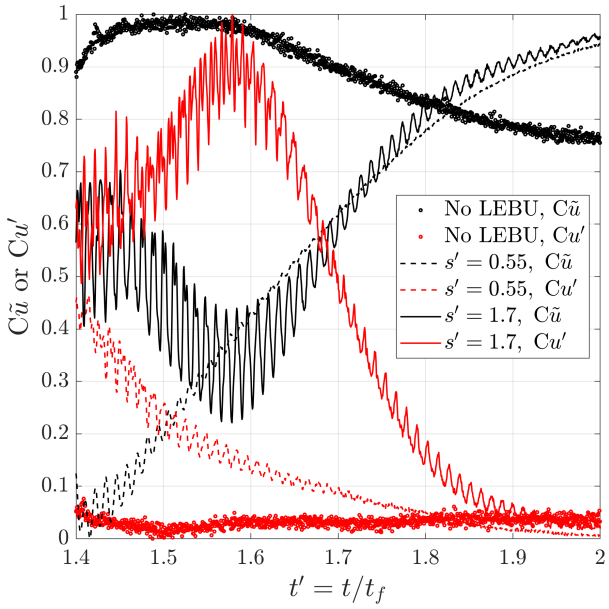

FIG. 10. Variations of the C$\tilde{u}$ and Cu' pertaining to the lower elongated streak behind the turbulent spot, as indicated by the arrows in Figure 9.

$$CT(y,t') = \frac{[T(y,t') - T_{\min}(y)]}{[T_{\max}(y) - T_{\min}(y)]}, \tag{3}$$

where T can either be $\tilde{u}$ or u'. The minimum and maximum values are determined from $1.3 \leq t' \leq 2.2$, which represent the temporal domain behind the turbulent spot where the elongated streaks are prominent. As shown in Figure 10, C$\tilde{u}$ and Cu' are anti-correlated against each other, but they both reveal the presence of unsteadiness and oscillation for the turbulent mixing layer behind the turbulent spot. This feature is persistent and becoming more prominent at larger s', thus resembling a vortex shedding phenomenon whose f', a non-dimensional shedding frequency normalised by the $U_\infty/\delta_{\text{spot}}$, is found to be close to 1. This means that the vortex shedding has a coverage of the entire height of the turbulent spot. The propagation of vortex shedding inside a boundary layer explains the two streams of $\pm\tilde{u}$ at the outer layer of the turbulent spot, and the elongated streaks that they entail. Due to the vortical shedding motion, the $+\tilde{u}$ is caused by the entrainment of higher momentum fluids from above. The opposite is true when the lower momentum fluids from below is drawn upwards to cause a $-\tilde{u}$.

Overall, the effect of the LEBU wake on the momentum distributions inside a turbulent spot seems to transpire at the outer layer only. The two elongated streaks are still relatively symmetrical when the LEBU is placed at $s' = 0.55$. It is also noticeable that a reduction of momentum excess at the leading edge overhang occurs.

The implications of the wake mixing to the spot's turbulence intensity characteristics can be found in Figure 9(b) and (c). First, turbulence level inside the leading edge overhang is suppressed. This indicates a reduced significance of wall bursting in the turbulence production. Second, turbulence level at the intermediate wall-normal distance ($0.2 < y/\delta_{\text{spot}} < 0.5$) also reduces across the main body. This is possibly due to the lack of wall bursting events at the leading edge that lead to a reduced turbulence level at the adjacent intermediate height region. Third, at a further height of $y/\delta_{\text{spot}} \approx 0.6$, direct interactions between the LEBU wake and the turbulent spot would produce dominant turbulent mixing layers with oscillatory behaviours (also shown in Figure 10). Finally, an enhanced wall turbulence layer appears at $y/\delta_{\text{spot}} < 0.2$, which is significantly larger than the baseline (no LEBU) level shown in Figure 7(b). Such an enhanced wall turbulence layer also coincides with the secondary deficit identified earlier in Figure 8(a).

To summarise the observations thus far, injecting a LEBU wake at a relatively close distance ($s' = 0.55$) and at the outer layer can re-distribute the turbulence and cause a non-equilibrium turbulent boundary layer. The emanated wake width is still relatively narrow owing to the close proximity of the LEBU, where wake oscillation in a form of vortex shedding is not strong enough yet to perturb the near wall region significantly. Combining these factors could imply that mitigation of the near wall turbulence cannot be achieved at this stage. Rather, a LEBU in close proximity can even enhance the turbulence level at the near wall region, and in turn cause an increase of the overall wall pressure fluctuations compared to the baseline case (Figure 6).

Contours of $\tilde{u}$, u' and $u'_{\text{baseline}} - u'_{\text{LEBU}}$ subjected to LEBU placement at $s' = 1.7$ are shown in Figure 9(d−f), respectively. The main consequence of a slightly displaced LEBU in the upstream direction is the enabling of wake growth inside a turbulent spot, which also results in an increasingly asymmetrical elongated streaks. From the velocity perturbation contour in Figure 9(d), the $+\tilde{u}$ streak becomes more dominant than the $-\tilde{u}$ counterpart owing to the variation in shear stress level as

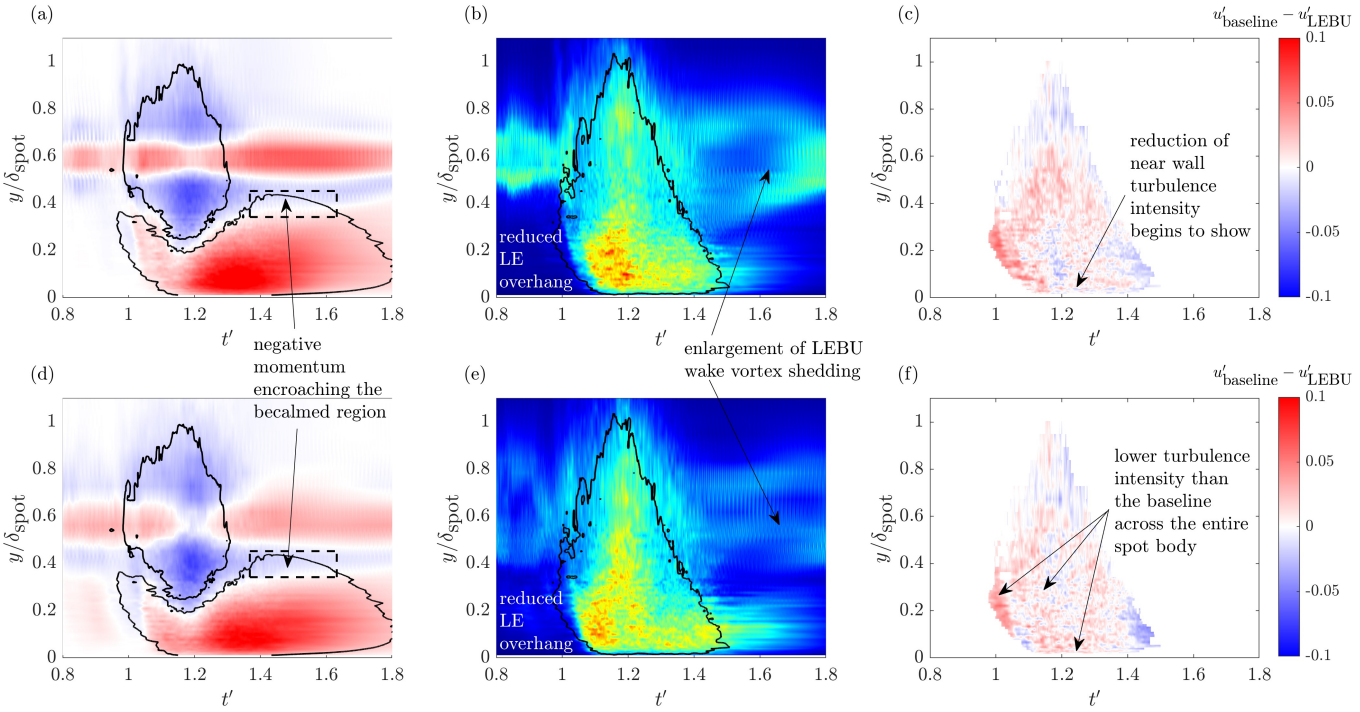

FIG. 11. Contours of the (a, d) velocity perturbation $\tilde{u}$, (b, e) turbulence intensity u' and (c, f) difference in turbulence intensity $u'_{\text{baseline}} - u'_{\text{LEBU}}$ at the plane of symmetry of a turbulent spot at $x = X_{\text{ref}}$. The LEBU is placed at $s' =$ (a−c) 3.3, and (d−f) 5.5. The outlines of the baseline (i.e. in the absence of LEBU) turbulent spot identified in Figure 7 are superimposed as black lines to the contours of (a, d) $\tilde{u}$ and (b, e) u'. Refer to Figure 7 for the colorbars of $\tilde{u}$ and u'.

a function of wall-normal distance across the boundary layer. The trajectory of the $-\tilde{u}$ streak is also found to be increasingly nudging downwards towards the wall, and approaching the boundary of the becalmed region of the baseline turbulent spot. This is an important phenomenon, which will be investigated further in the next section.

As demonstrated in Figure 9(e), the turbulent mixing layers are now considerably thicker, and also extended beyond the boundaries of the baseline turbulent spot both in the front and aft regions. The suppression of leading edge overhang, hence the wall bursting event in turbulence production, continues to happen here. The emergence of enhanced vortex shedding in this case, as demonstrated in Figure 10, further disrupts the turbulence distribution within a turbulent spot via an *entrainment* process. The entrained turbulent fluids will then be propagating at a lower speed than the turbulent spot as their bulk convection is now dictated by the wake vortex. As demonstrated in Figure 10, the different convection rates can shift the turbulence peak Cu' and the momentum trough C$\tilde{u}$ at the outer layer to $t' = 1.58$, which is equivalent to outside of the baseline turbulent spot boundary in the spatial domain.

Although placing the LEBU at $s' = 1.7$ is effective in the mitigation of turbulence level at the outer layer, it still generates high level of turbulence at the near wall region (see Figure 9f). Such characteristic indeed correlates well with Figure 6 where the measured overall wall pressure fluctuations level subjected to interaction with LEBU is still higher than that of the baseline case.

D. Interactions between the LEBU wake and turbulent spots at $s' > 3$

It is important to remind again that the LEBU wake is only visible in the ensemble-averaged contours when it has become a tracer, which entails mixing with the turbulent spot and transporting its momentum and turbulence. Therefore, any residues of the $\tilde{u}$ and u' that occur outside the boundary of the baseline turbulent spot, as shown extensively in Figure 11(a−b, and d−e) when in both cases representing $s' > 3$, have reflected a significantly distorted turbulent spot structure due to the thickened LEBU wake. The dominant vortex shedding remains a main feature that will be demonstrated later. Due to the increased wake width of the LEBU, it is encompassing a greater spatial coverage within the spot's main body, thus exerting a greater effect.

The impact of larger LEBU wake distortion to the turbulent spot can first be examined from the velocity perturbations. At $s' = 3.3$ in Figure 11(a), the two elongated streaks become even more asymmetrical. The streak that corresponds to the $-\tilde{u}$ has partially immersed in the becalmed region of the otherwise baseline turbulent spot. At $s' = 5.5$ in Figure 11(d), the $-\tilde{u}$ streak is displaced further more towards the becalmed region. As discussed in Section IV A, the becalmed region is formed by the downstream 'sweeping' of high momentum fluid from the freestream towards the turbulent spot's trailing edge. This represents the physical mechanism that a high $+\tilde{u}$ is always established behind a turbulent spot. When a

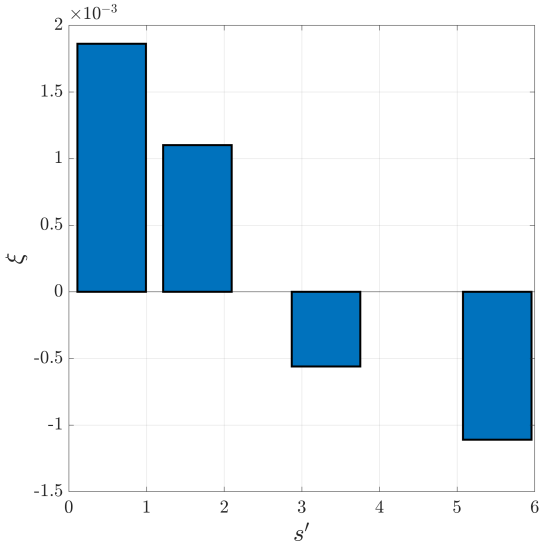

FIG. 12. Distribution of ξ against s'.

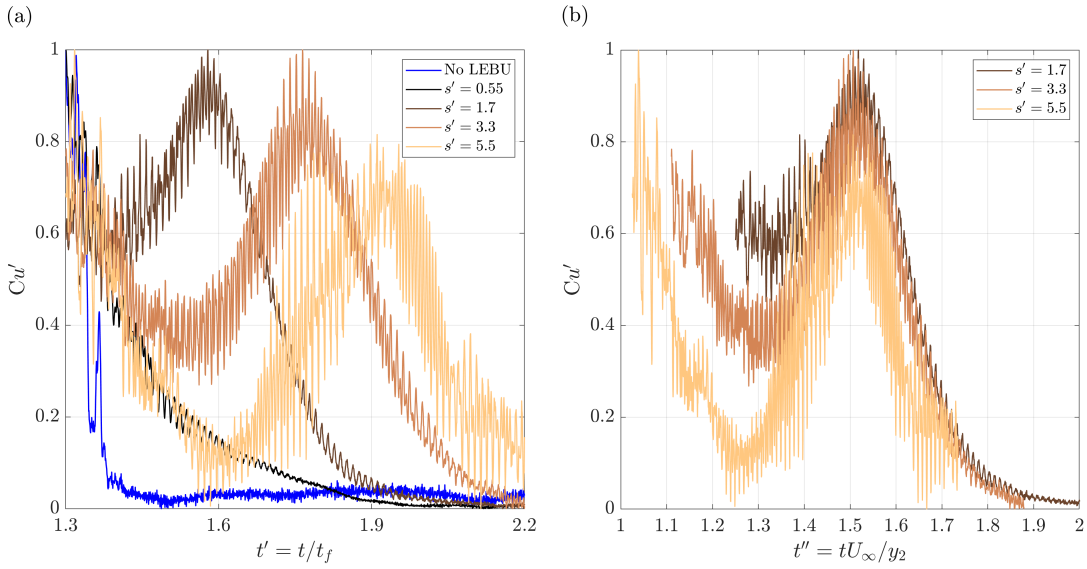

FIG. 13. Variations of Cu' against (a) t' and (b) t'', for different s'.

LEBU wake of $-\tilde{u}$ is increasingly encroaching the becalmed region, it will inhibit the sweeping event and disrupt the entire turbulence re-generation cycle. To provide evidence for this, a spatial-temporal integration for the velocity perturbation is performed at the becalmed region just outside the turbulent spot's trailing edge, which is marked by the dashed-boxes as depicted in Figure 9(a, d) and Figure 11(a, d), to produce:

$$\xi = \int\int \tilde{u}\,\mathrm{d}(t')\,\mathrm{d}(y/\delta_{\mathrm{spot}}). \tag{4}$$

As shown in Figure 12, a high positive ξ is initially achieved at $s' = 0.55$. ξ will be reduced, albeit still retaining positive level, when s' increases to 1.7. The trend continues, during which ξ switches to negative at $s' \approx 3$. Further increases of s' beyond 3 will produce larger negative values of ξ.

When the ξ becomes negative, the wall sweeping will be inhibited. On the other hand, the ability of the LEBU wake to destroy the leading edge overhang, which is formed by the wall bursting, continues to feature here. This suggests that the burst-and-sweep cycle needed for the sustainability of a turbulent boundary layer have been simultaneously disrupted when $s' > 3$. As shown in Figure 11(c, f), a significant reduction of the turbulence intensity level can be found almost across the entire turbulent spot, including at the near wall region. The successful suppression of the entire turbulence level when $s' > 3$ correlates well with the corresponding reduction of the overall wall pressure fluctuations in Figure 6.

As shown in Figure 13(a), Cu' at the mixing outer layer decays exponentially against t' when $s' = 0.55$. When the s'

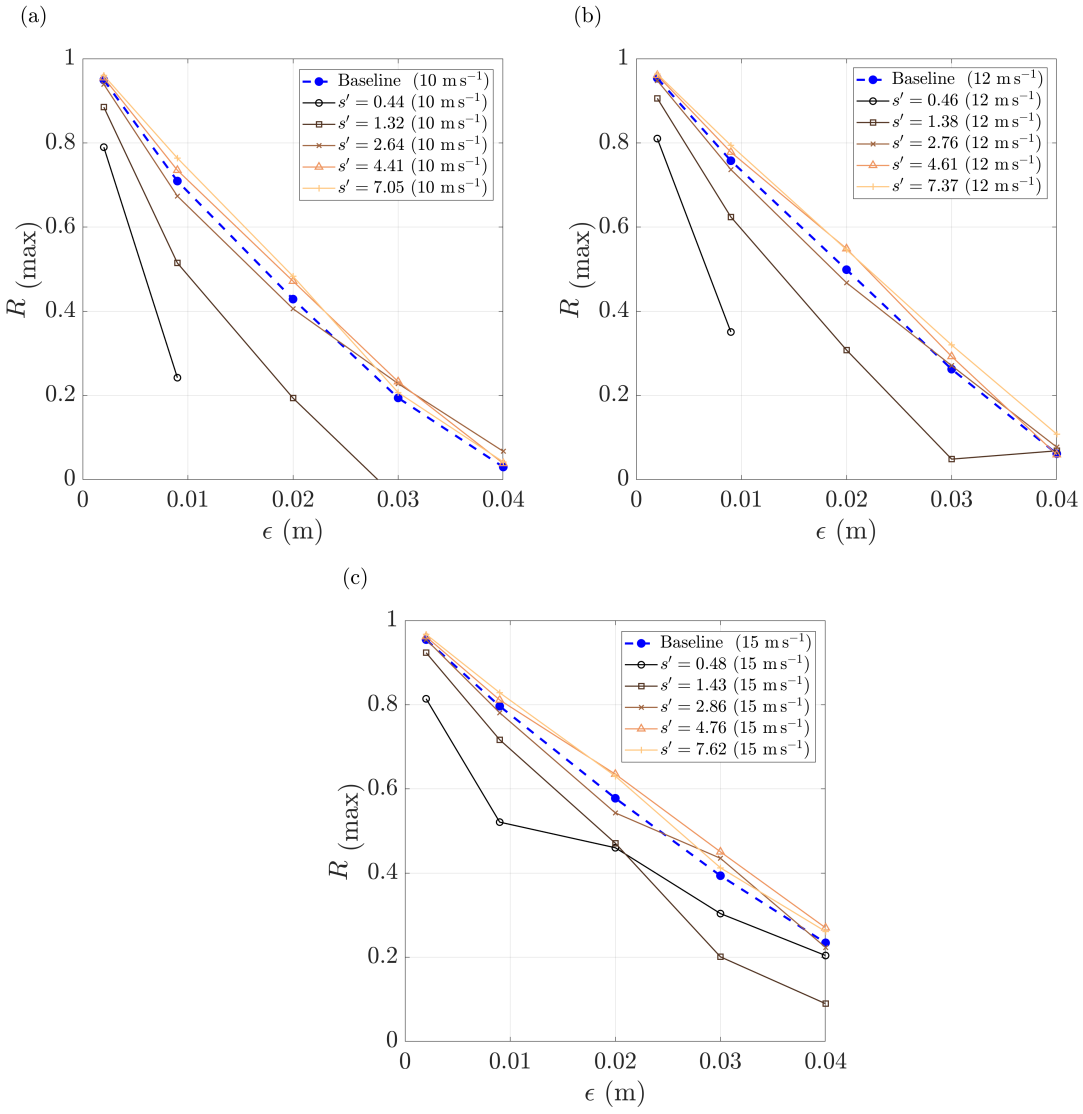

FIG. 14. Distributions of the maximum cross-correlation coefficients for the wall pressure fluctuations, $R_{x_i x_j\,(\max)}$ against ϵ for U_∞ = (a) 10 ms^{-1}, (b) 12 ms^{-1} and (c) 15 ms^{-1} across $0.44 \leq s' \leq 7.62$.

gradually increases, the corresponding Cu' will start to exhibit a single pulse-liked response superimposed by prominent high-frequency fluctuations that reflect the vortex shedding phenomenon. As s' increases, the turbulence level of the peaks will be reduced, and most importantly, the time of occurrence for the peaks t_{peak} will increase. As discussed in the previous section, the peak is associated with the entrained turbulent fluids from the wall, which is then convecting at a lower speed than the turbulent spot at the outer layer.

Hence, one could establish the relationship between the t_{peak} and the LEBU placement s. Applying the normalisation factor s/U_∞ directly, however, is unable to collapse the t_{peak} because the changes in s are several magnitude of order larger than the changes in t_{peak} under a constant freestream velocity U_∞. Instead, the wall-normal distance of the secondary deficits y_2 (defined in Section IV B), which is found to yield a relationship of $y_2/\delta_{\text{spot}} \propto 0.0052s'$, is found to be a suitable surrogate. A new definition of the non-dimensional time scale, $t'' = tU_\infty/y_2$, can indeed collapse the Cu' for $1.7 \leq s' \leq 5.5$ very well, as demonstrated in Figure 13(b). This means that the ability to separate the entrained wall turbulent fluids from the turbulent spot, which should be beneficial in the mitigation of the wall pressure fluctuations, is correlated to the wall-normal distance of the secondary deficit that is ultimately governed by s.

V. WALL TURBULENCE CHARACTERISTICS AT $x > X_{\text{ref}}$

Studying the interaction between the turbulent spots and LEBU wake in Section IV has provided some plausible explanations for the cause of the self-similarity behaviour in the

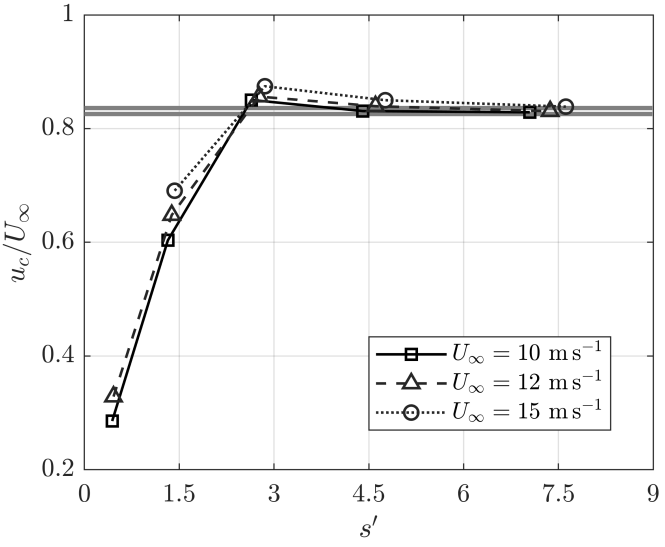

FIG. 15. Convection velocities of the most dominant turbulence eddies as a function of s' at U_∞ = 10, 12 and 15 m s^{-1} in the presence of LEBU. The datum range produced by the baseline flat plate is indicated by the thick horizontal lines.

wall pressure fluctuation with respect to s'. In this section, the focus will return to the canonical case when the turbulent boundary layer is generated by a passive tabulator in the same setup as Section III, and the loudspeaker used to generate turbulent spots disconnected. More specifically, we will investigate the influence of LEBU wake to the wall turbulence at $x > X_{\text{ref}}$.

As already described in our earlier paper[5], in addition to the reference microphone at X_{ref}, the flat plate system also contains extra surface microphones at $x > X_{\text{ref}}$, up to $x = 725$ mm. It is worth mentioning that the wall pressure spectra measured at $x > X_{\text{ref}}$ also follow the self-similarity rule described in Section III. The results have been discussed elsewhere[24] and will not be included here for brevity.

In total, eight microphones at $625(X_{\text{ref}}) \leq x \leq 725$ mm are measured simultaneously, which allow cross-correlation study in the spatial-temporal domain to be conducted. The output of this analysis is normally the cross-correlation coefficient $R_{x_i x_j}$ as a function of time delay between the signals, τ. Note that the cross-correlation coefficients are non-dimensionalised to result in a range of $0 \leq R_{x_i x_j} \leq 1$. All the streamwise cross-correlation studies were conducted by taking reference to X_{ref}, which give rise to $\varepsilon = x - X_{\text{ref}}$. The decay of the most dominant wall pressure generating structures can thus be examined by identifying the maximum cross-correlation coefficient $R_{x_i x_j(\max)}$ at each ε. Figure 14 plots the distributions of $R_{x_i x_j(\max)}$ against ε for a range of s' at U_∞ = 10, 12 and 15 m s^{-1}. The baseline case, i.e. in the absence of LEBU, is also included in the figure.

A common feature in Figure 14 is the very fast decay rate of $R_{x_i x_j(\max)}$ when s' is very low. At $s' = 0.44 - 0.48$, the decay of $R_{x_i x_j(\max)}$ is so fast that in some cases it has become indiscernible at $\varepsilon > 0.01$ m. This phenomenon is attributed to the imposition of the self-similarity rule that forces the mechanism underpinning the generation of the most dominant wall pressure structure at X_{ref}, which can produce very high level of wall pressure fluctuations (see Figure 5), to be destroyed quickly.

At $s' = 2.64 - 2.86$, the distributions of $R_{x_i x_j(\max)}$ against ε is very similar to their baseline counterparts. Further increase of s' to between 4.41 and 7.62 will even help to preserve the $R_{x_i x_j(\max)}$ against ε slightly better than the baseline. This is an encouraging result because it means that the dominant mechanism for the wall pressure fluctuations at X_{ref} and $s' > 3$, which will not be as effective as the baseline in the production of the wall pressure fluctuations, can maintain its low turbulence wall pressure characteristics over a large streamwise distance.

The convection velocity of the most prevalent turbulence scale and dominant wall pressure generating turbulence structures to traverse from X_{ref} to $X_{\text{ref}} + \varepsilon$ can be identified by the $\tau_{(\max)}$ corresponding to the maximum cross-correlation coefficient $R_{x_i x_j \max}$. From a dataset of $(\varepsilon, \tau_{\max})$, an average convection velocity for the dominant large scale turbulent eddies can be determined. It should be noted that the most dominant turbulent eddies in the boundary layer would decay at a slower rate than the small-scale turbulent eddies.

Figure 15 shows the normalised convection velocities of the turbulence eddies u_c/U_∞, as a function of s', at U_∞ = 10, 12 and 15 m s^{-1}. The datum range produced by the baseline flat plate in the absence of LEBU is indicated by the thick horizontal lines. The remarkably close resemblance between this figure and Figure 6 for the $10\log_{10}(S_{qqb}/S_{qql})$, both of which would demonstrate the $s' = 3$ as the threshold for significant changes in the wall pressure fluctuation and turbulence convection, is noteworthy. Figure 15 demonstrates that the LEBU can slow down the longitudinal turbulence convection initially. The deviation from the baseline datum is the most significant at low s', i.e. when the LEBU is at the closest proximity to X_{ref}. This illustrates that the velocity deficit of the near wake emanated from the LEBU can exert a re-

tarding impact to cause a significant slow down of the local turbulence convection. For example, a reduction of u_c/U_∞ to approximately 0.3 at $s' = 0.44 - 0.48$ is observed. However, as s' increases, the turbulence convection will undergo a steep recovery to return to the baseline datum. A slight overshoot in the turbulence convection appears at $2.5 \leq s' \leq 4.5$, before returning to the baseline level at $s' > 5$. Figure 15 thus provides a clear indication that the LEBU is capable of disrupting the turbulence convection considerably.

VI. OUTLOOK

The robustness of $s' = 3$ as the critical value to determine enhancement or suppression of the turbulent wall pressure by LEBU wake could be affected by other influencing parameters, such as the wall-normal position of the LEBU, $\tilde{h}$, as well as the aerofoil shape and size of the LEBU (e.g. C_{LEBU}). In our previous study[24] where the same LEBU is placed very close to the wall surface to target the inner part of the turbulent boundary layer, the close proximity of the LEBU wake to the wall surface will inadvertently enable a direct addition of low frequency hydrodynamic pressure fluctuations emitted from the LEBU wake to the wall surface. This process will enhance the low frequency wall pressure fluctuations. Subsequently, the wall pressure spectra will not feature a self-similarity behaviours against the s'. Nevertheless, when the LEBU is placed sufficiently away from the wall surface such that its emanated wake will be targeting the outer part of turbulent boundary layer downstream, self-similarity should be established robustly. The effect of C_{LEBU} on the LEBU wake width, and how it might affect the optimal s', is not considered here though it could be studied in the future.

This paper only considers a canonical flat plate configuration where the boundary layer was generated on zero pressure gradient flow. In many real life applications, transient flow conditions can change the boundary layer characteristics at the target reference location quite rapidly and significantly. To improve the versatility of the LEBU, the angle of attack of the LEBU relative to the wall surface (α_{LEBU}) can be included as one of the performance parameters to ensure that optimal s' is always maintained. This can be achieved by designing the α_{LEBU} as an active control parameter to match the various operation conditions of the target blade.

VII. CONCLUDING REMARKS

Even a fully developed turbulent boundary layer can still be perturbed by external disturbances, which could result in either an enhancement or suppression of its velocity and wall pressure fluctuation fields. In this paper, we used a two-dimensional, Large Eddy BreakUp (LEBU) device in the form of scaled-down NACA0014 aerofoil, and exploited the emanated wakes to target the outer part of a turbulent boundary layer developed on a flat plate. Rather than focusing on the LEBU's capability in the turbulent skin friction reduction, this paper aims to use LEBU to mitigate the wall pressure fluctuations, which are considered as the main hydrodynamic sources for the trailing edge noise and turbulent boundary layer noise radiations.

One of the objectives for this work is to establish the optimal s', and its responses to some of the influencing parameters. Here, $s' = s/\delta_\circ$, where s is the separation distance between the LEBU's trailing edge and the targeted location for noise mitigation, and $\delta_\circ$ is the boundary layer thickness at the targeted location. When a LEBU is placed at a wall-normal distance corresponds to the outer part of a turbulent boundary layer, and at $s' < 3$, the emanated wake can retard the large scale turbulence convection rates significantly. The threshold of $s' = 3$ is accurately replicated in the wall pressure turbulence, which has exhibited a high level of self-similarity behaviours. A retardation of the large scale turbulence convection rates that occurs at $s' < 3$ will coincide with the production of wall pressure fluctuation whose level is higher than the baseline case in the absence of LEBU. However, further upstream placement of the LEBU beyond the threshold, i.e. $s' > 3$, can result in a steep recovery of the large scale turbulence convection rates to reach the baseline datum, which is now accompanied by a reduction in the wall pressure level when compared to the baseline case.

A study on the velocity field, from the perspective of turbulent spots, demonstrates a consistent presence of enhanced near wall turbulence at $s' < 3$, which manifests into high level of wall pressure fluctuations. This causal effect would replicate, albeit reversely, when $s' > 3$. At this sufficiently large separation distance, the wake interaction entails a significant reduction of the velocity turbulence intensity across the entire structure of turbulent spot, including the near wall region. Consequently, the wall pressure fluctuation is also reduced. There is a high degree of correlation between the unsteady velocity in the boundary layer and the underlying turbulent wall pressure.

After the interaction between the emanated LEBU wake and outer part of turbulent spot, an oscillated mixing fluids with a regular periodicity that resembles a vortex shedding behaviour is generated. In general, this interaction can introduce a *pressure shielding* effect, which is regarded as an effective mechanism for the interruption of turbulence re-generation by inhibiting the sweeping and ejection events of the coherent structures. Some of which have indeed been manifested in the turbulent spots in a straightforward fashion, where the leading edge overhang has been consistently suppressed across the entire range of s' investigated here. Leading edge overhang is formed after the ejected turbulent fluids, which has no re-generation mechanism outside the boundary layer, decay and join the nose. However, the wall pressure fluctuations become higher and lower than the baseline levels at $s' < 3$ and $s' > 3$, respectively. This means that the disruption of the ejection event alone may not be adequate for the wall pressure mitigation.

The pressure shielding effect, and its ability to reduce wall pressure fluctuation, can only become fully effective when the sweeping event is also disrupted. Results show that this can only be realised at $s' > 3$ when the oscillated mixing layer

has grown a considerable width such that it inhibits the momentum required to facilitate the sweeping event near the becalmed region, behind the turbulent spot's trailing edge. Indeed, the turbulence intensity within the entire turbulent spot, including its near wall region, is reduced significantly when $s' > 3$. In summary, there exists a high correlation between the wall pressure fluctuation on a turbulent boundary layer, and the velocity fluctuations on a turbulent spot, where both have the same responses against the s'.

ACKNOWLEDGMENT

This research was funded, in whole or in part, by the Engineering and Physical Sciences Research Council in the United Kingdom through research grant No. EP/K002309/1. A CC BY or equivalent licence is applied to the Author Accepted Manuscript arising from this submission, in accordance with the grant's open access conditions. The authors would also like to thank the PhD studentship sponsored by the Thomas Gerald Gray Charitable Trust in the United Kingdom.

AUTHOR DECLARATIONS

The authors have no conflicts to disclose.

DATA AVAILABILITY

The data that support the findings of this study are available from the corresponding author upon reasonable request.

[1]M. S. Howe. Aerodynamic noise of a serrated trailing edge. *J Fluid Struct*, 5(1):33–45, 1991.

[2]B Lyu, M Azarpeyvand, and S Sinayoko. Prediction of noise from serrated trailing edges. *J Fluid Mech*, 793:556–588, 2016.

[3]P. C. Woodhead, T. P. Chong, P. F. Joseph, J. G. Wissink, and P. Chaitanya. Frequency-targetable aerofoil self-noise reduction. In *27*th *AIAA/CEAS Aeroacoustics Conference*, AIAA 2021-2229 paper, Washington DC, 2021.

[4]M. M. Scholz, T. P. Chong, and E. Smith. New strategy on porous trailing edge for self-noise reductions. In *27th AIAA/CEAS Aeroacoustics Conference*, AIAA Paper 2021-2109, Washington DC, USA, 2021.

[5]Chioma Muhammad and Tze Pei Chong. Mitigation of turbulent noise sources by riblets. *Journal of Sound and Vibration*, 541:117302, 2022.

[6]I. A. Clark, W. N. Alexander, W. J. Devenport, S. A. L. Glegg, J. W. Jaworski, C. A. Daly, and N. Peake. Bioinspired trailing-edge noise control. *AIAA J*, 55:740–754, 2017.

[7]A. Gonzalez, S. A. L. Glegg, N. Hari, M. Ottman, and W. J. Devenport. Fundamental studies of the mechanisms of pressure shielding. In *25th AIAA/CEAS Aeroacoustics Conference*, AIAA Paper 2019-2403, Delft, The Netherlands, 2019.

[8]P. H. Alfredsson and R. Örlü. Large-eddy breakup devices – a 40 years perspective from a stockholm horizon. *Flow, Turbulence and Combustion*, 100:877–888, 2018.

[9]P.R. Spalart, M. Strelets, and A. Travin. Direct numerical simulation of large-eddy-break-up devices in a boundary layer. *International Journal of Heat and Fluid Flow*, 27(5):902–910, 2006.

[10]K. S. Yajnik and M. Acharya. Non-equilibrium effects in a turbulent boundary layer due to the destruction of large eddies. In H. Fiedler, editor, *Structure and Mechanisms of Turbulence I*, pages 249–260, Berlin, Heidelberg, 1978. Springer Berlin Heidelberg.

[11]J. N. Hefner, L. M. Weinstein, and D. M. Bushnell. *Large-Eddy Breakup scheme for turbulent viscous drag reduction*, pages 110–127. 1980.

[12]A. M. Savill and J. C. Mumford. Manipulation of turbulent boundary layers by outer-layer devices: skin-friction and flow-visualization results. *Journal of Fluid Mechanics*, 191:389–418, 1988.

[13]T. P. Chong and A. Juknevicius. Reconstruction of the deterministic turbulent boundary layer for the study of aerofoil self-noise mechanisms. *Exp Fluids*, 63:139, 2022.

[14]M. Roger and S. Moreau. Broadband self noise from loaded fan blades. *AIAA J.*, 42(3):536–544, 2004.

[15]A. P. Garcia Sagrado. *Boundary layer and trailing edge noise sources*. PhD thesis, University of Cambridge, 2008.

[16]M. Gruber. *Airfoil noise reduction by edge treatments*. Phd thesis, University of Southampton, 2012.

[17]I. Wygnanski. The effects of reynolds number and pressure gradient on the transitional spot in a laminar boundary layer. In J. Jimenez, editor, *The Role of Coherent Structures in Modelling Turbulence and Mixing*, pages 304–332, Berlin, Heidelberg, 1981. Springer Berlin Heidelberg.

[18]A. Glezer, Y. Katz, and I. Wygnanski. On the breakdown of the wave packet trailing a turbulent spot in a laminar boundary layer. *J Fluid Mech*, 198:1–26, 1989.

[19]T. P. Chong and S. Zhong. On the momentum and thermal structures of turbulent spots in a favorable pressure gradient. *J Turbomach*, 128(4):689–698, 2006.

[20]T. P. Chong and S. Zhong. On the three-dimensional structure of turbulent spots. *J Turbomach*, 127(3):545–551, 2005.

[21]G. B. Schubauer and P. S. Klebanoff. Contributions on the mechanics of boundary-layer transition. Nasa reference publication 1289, retrieved from: https://ntrs.nasa.gov/api/citations/19930092285/downloads/19930092285.pdf, NASA Langley Research Center, Hampton (VA), 1956. (Accessed: 2021-07-05).

[22]J. P. Gostelow, N. Melwani, and G. J. Walker. Effects of streamwise pressure gradient on turbulent spot development. *J Turbomach*, 118(4):737–743, 1996.

[23]Mohamed Gad-El-Hak, Ron F. Blackwelderf, and James J. Riley. On the growth of turbulent regions in laminar boundary layers. *J Fluid Mech*, 110:73–95, 1981.

[24]C. Muhammad and T. P. Chong. Perturbation of turbulent boundary layer by outer layer and inner layer devices for turbulent noise source reduction. In *29*th *AIAA/CEAS Aeroacoustics Conference*, AIAA 2023-3336 paper, 2023.